CORONOGRAPHY STUDY FOR HYPERTELESCOPE

S. Gillet[1], P. Riaud[2], A. Boccaletti[2], L. Arnold[4], O. Lardière[3], V. Borkowski[1], and A. Labeyrie[1,3]

[1]L.I.S.E. Observatoire de Haute Provence 04870 Saint Michel l'Observatoire
sgohp@obs-hp.fr, labeyrie@obs-hp.fr, borkowski@obs-hp.fr
[2]L.E.S.I.A. Observatoire de Meudon Place Jules Janssen, F-92195 Meudon Cedex
pierre.riaud@obspm.fr, anthony.boccaletti@obspm.fr
[3]Collège de France, 11 place Marcelin Berthelot, 75005 Paris
dejonghe@obs-hp.fr, lardiere@obs-hp.fr
[4]O.H.P. Observatoire de Haute Provence 04870 Saint Michel l'Observatoire
arnold@obs-hp.fr

ABSTRACT

Following the idea developed in (Boccaletti et al. 2000), a snapshot imaging interferometer is proposed as an alternative to the NASA Origin project: "Terrestrial Planet Finder". This concept is based on densified pupil imaging (Labeyrie 1996) and phase-mask coronagraphy by (Rouan et al. 2000). The so-called Four-Quadrant Phase-Mask features a large starlight attenuation (10^{-8}). Thorough calculations indicate that the detection of Earth-like planets amidst zodiacal and exo-zodiacal clouds is faster with an imaging system than with a nulling interferometer as originally proposed for the TPF design. Detailed numerical simulations have been carried out taking into account several sources of noise and as a result we found that Earth-like planets can be imaged up to about 25 pc with a large interferometer in the thermal infrared. Finally this concept seems promising for discovering life hints with medium resolution spectra in both the visible (O_2, CH_4, H_2O and Chlorophylla signature) and the thermal infrared (CH_4, H_2O, O_3, CO_2, NH_3).

Key words: hypertelescope, coronagaphe, exoplanets, TPF, nulling interferometer.

1. INTRODUCTION

This article describes our recent progress in the study of the hypertelescope-coronograph concept for the detection and observation of Earth-like planets, the challenging goal of NASA's Terrestrial Planet Finder (TPF hereafter) space mission. Hypertelescope provides the possibility of observing direct high resolution images with an interferometer (Labeyrie 1996). Previous calculations (Boccaletti et al. 2000) have shown that this concept improves noticeably the detection capabilities of exo-planets, compared to the initial instrument concept, based upon the idea of a nulling interferometer according to Bracewell's option (Bracewell 1978; Bracewell 1979). We present here more realistic numerical simulations, incorporating several sources of noise that were not accounted for in our earlier simulations (Boccaletti et al. 2000), i.e. mainly the zodiacal and exozodiacal contaminations but also co-phasing errors among the sub-apertures and the thermal emission of mirrors. These simulations are performed with a new version of the phase-mask coronagraph (Rouan et al. 2000), the Four-Quadrant Phase Mask, which improves significantly the detection of faint circumstellar sources (Riaud et al. 2001) with respect to the former Roddier's phase-mask (Roddier et Roddier 1997). We present briefly the concept of hypertelescope in section 2. Section 3 presents the different sources of noise taken into account and we finally discuss the theoretical results of exo-planets detectability.

2. HYPERTELESCOPE PRINCIPLE

A hypertelescope or also pupil densified interferometer is a imaging interferometer which performs snapshot images. The principle was previously described (Labeyrie 1996; Boccaletti et al. 2000; Riaud et al. 2002). Unless the use of noiseless detectors, densifying the pupil allows to take high resolution snapshot images. The dilated mirrors forming a so-called Fizeau interferometer, are optically put together and form a densified pupil, provided that the pattern formed by the center of the sub-pupils is kept with no changing. The relationship between the object O on the sky and its image I is given by :

$$I = [O \otimes Int] * W \quad (1)$$

Proc. ESLAB 36 Symposium, 'Earth-Like Planets and Moons', ESTEC, Noordwijk, 3-8 June 2002 (ESA SP-514, October 2002)

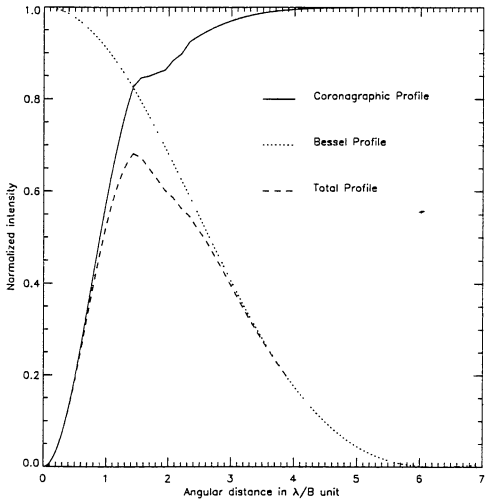

Figure 1. Attenuation of a planet by the coronagraph (solid) and the diffractive envelope ZOF (dotted) as a function of the angular separation (λ/B unit). The maximal transmission is achieved at 1.4 λ/B. However, the planet light lost from the zero-order image due to the envelope's attenuation finds its way into the first-order images appearing at known relative positions within the envelope.

Int is the interference function, Fourier transform of the apertures. W, the windowing function, defines the hypertelescope's field of view, also called the ZOF (Zero Order Field) and is the Fourier transform of an exit sub-pupil. In case of circular sub-apertures, the windowing function $W(\theta)$ is an Airy pattern and the ZOF in the high-resolution image corresponds to the first dark ring. Unlike the Fizeau interferometer and its infinite field of view, the pupil densification shrinks the field according to W while intensifying the part of the interference function appearing within the diffractive envelope. However, a star located outside the ZOF but inside a region called the HOF (High Order Field) provides an interference peak inside the ZOF, but with a radial dispersion in polychromatic light. Thus, the HOF, larger than the ZOF, and defined by $HOF = \lambda/d$ where d is the entrance mirror diameter, is taken into account for the detection calculation of exoplanets hereafter presented in section 3.

We consider here a hypertelescope with 37 hexagonal sub-apertures, placed on free-flyers, and located on a spherical surface according to a periodic hexagonal pattern, suitable for full densification in the exit pupil. A coronagraphic device is attached to the hypertelescope imager for attenuating the central star and detecting the possible planet's image. We considered, among a wide range of coronagraphs, the Four-Quadrant Phase-Mask (FQ-PM hereafter) (Rouan et al. 2000; Riaud et al. 2001) which appears to be the most efficient coronagraph concept in terms of star light rejection. The FQ-PM is assumed to be perfectly achromatic and the hypertelescope has no central obscuration, which is achievable in practice by slightly off-setting the combiner optics at the focus of a large diluted mosaic mirror, whether paraboloidal or spherical.

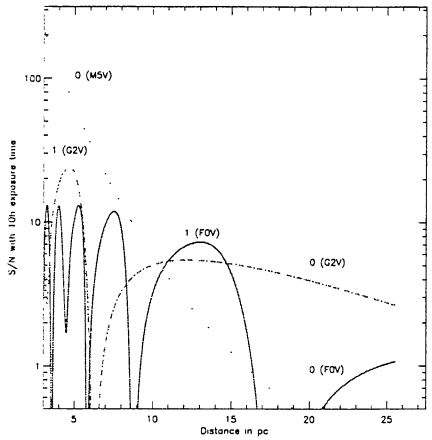

Figure 2. Signal to noise ratio obtained in 10 hours for stars of spectral type F0V (solid), G2V (dash-dotted) and M5V (dotted) assuming a baseline of 80m and versus the distance in parsec. Earth-like planets are detectable in order 0 for M5V stars, in order 0 and 1 for G2V stars, and in orders 1 to order 5 for F0V stars. (Hipparcos).

3. NUMERICAL SIMULATIONS

Several sources of noise have to be taken into account when observing an infra-red signal from an extra-terrestrial planet orbiting around a bright star. The major source of noise is the residual star's light and, to a lesser extent, the speckle noise originating from phase aberrations in the optical train (cophasing defects or mirror roughness). We also take into account the attenuation by the coronagraph on both the star and the planet and the transmission by the ZOF envelope (Fig.1). Each flux is calculated in a resel λ/B. Table 1 list the different sources of noise which are contaminating the exo-planet peak in the densified-pupil image at a θ angular distance from the star, with J_p photo-events detected per second and per resolution element (resel) for the planet.

Including the different sources of noise, the S/N can be written as :

$$S/N = \frac{J_p.t}{\sqrt{(\sum_i J_i.t + N_{dark} + N_{ron})}} \qquad (2)$$

Eq. 2 is also valid for a Fizeau interferometer since it has the same planet/background contrast. However, the hypertelescope provides the same S/N in a

shorter time since its sensitivity is largely improved by the pupil densification which intensifies the interference peak in the general case where the detector have readout noise and dark current.

One of the questions concerns S/N ratio of a planet located in the "habitable zone" i.e. with an effective temperature $Tp \approx 300K$. This "habitable zone" depends on the spectral type of the star which has to be taken into account. In order to have the largest sample of target stars, since the ZOF is very small ($\sim 12\lambda/B$ in diameter), it is important to exploit the higher-order dispersed peaks of a planet lying outside the ZOF to allow the detection of terrestrial planets for any type of stars and at any distances. Table 2 gives the flux remaining in the dispersed peaks when the bandwidth is reduced to accomodate the peak dispersion (in one resel) from order 0 (inside the ZOF) to order 7. As the planet moves away from the ZOF, the flux per resel of a higher-order peak decreases linearly owing to the spectral dispersion, while the planet's intrinsic luminosity varies as the inverse square of its distance to the observer. As a consequence, for a given spectral type, the S/N of a terrestrial planet located in the HOF is larger than in the ZOF (as seen on Fig. 2 for the F0V type).

Figure 2 shows the S/N estimated from Eq. 2 for stars belonging to 3 spectral types (F0V, G2V and M5V) located at any distance up to 25pc. The planet peak (whatever the order of the peak) is attenuated by the windowing function towards the edge of the ZOF and by the coronagraph towards the center of the field, as apparent in the S/N profiles presented in Fig. 2. Therefore, given the star's distance and spectral type the detection is optimal for a specific order. In the case of Fig. 2, Earth-like planets are detectable in order 0 for M5V stars, in order 0 and 1

Noise	Definition
$J_s(\theta)$	background from the residual starlight
$J_z(\theta, T_z)$	background from the zodiacal cloud with a temperature of T_z
$J_{ez}(\theta)$	background from the exo-zodiacal cloud
$J_{sn}(\theta)$	speckle noise of the residual starlight
$J_{id}(\theta, T_c)$	background from interstellar dust clouds with a temperature of T_c
$J_m(\theta, T_m)$	background from the mirror optical emissivity with a temperature of T_m
J_{conf}	confusion noise from background stars in the HOF
A_C	attenuation by the coronagraph
A_{HT}	attenuation by the windowing function
N_{dark}	thermal noise from the focal plane array (FPA)
N_{ron}	readout noise from the FPA
QE	quantum effiency of 45% (Rockwell Si:As detector)
T_O	optical transmission of 46%
T_F	filter transmission of 45% (N band $10.2 \pm 2\mu m$)

Table 1. Sources of noise budget

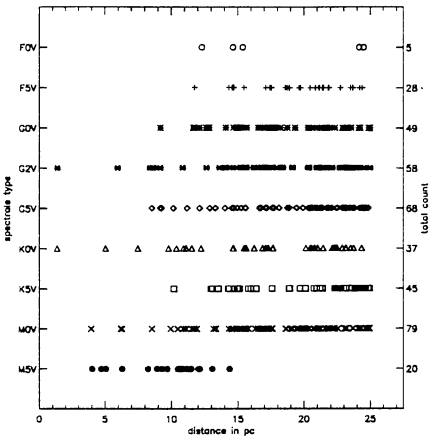

Figure 3. Distribution of stars closer than 25 pc for only nine spectral types (M5V to F0V). The vertical scale at left gives the spectral type and at right the total number of stars for each spectral type. For the whole sample of 389 stars, the distances and spectral types were obtained from the Hipparcos catalogue (Hipparcos).

order	0	1	2	3
Flux in %	100	98.5	85.5	66.4
Flux (spectrum) in %	86	84.3	74	56.4
λ_{min} in μm	6	7.65	8.5	8.925
λ_{max} in μm	14	12.75	11.9	11.475
order	4	5	6	7
Flux in %	53.2	44.3	38.1	32.9
Flux (spectrum) in %	43.9	35.6	30.8	26.6
λ_{min} in μm	9.18	9.35	9.47	9.56
λ_{max} in μm	11.22	11.05	10.93	10.08

Table 2. Flux of interference peaks at $\lambda = 10\mu m$ and the corresponding wavelength range ($\lambda_{max} - \lambda_{min}$) integrated in one resel.

for G2V stars, and from order 1 to order 5 for F0V stars.

The theoretical S/N obtained at $\lambda = 10\mu m$, for a sample of 389 main-sequence stars (M5, M0, K5, K0, G5, G2, G0, F5 and F0) contained in the Hipparcos catalog (ESA, 1997) (see Fig.3), is shown on Fig.4a and 4b with respectively a zodiacal flux of $10.8 mag/"^2$ (median value) and $13.0 mag/"^2$ (median value at the ecliptic pole). We assume a baseline of 80m, 10h of integration time and an exo-zodiacal cloud 10 times brighter than the zodi. As expected, the number of potentially detectable planets is considerably affected by the intensity of the zodiacal cloud. The S/N can be larger than 10 for stars closer than 15 pc and as large as $\sim$ 300 for a nearby for

nearby G2V and K0V stars (α Centauri). In the favorable case (Fig.4b), terrestrial planets could be detected around 67% of stars in our sample. This first sample of stars is of course biased by the selection of only 9 spectral types but was useful to investigate the optimal baseline and the effect of the zodiacal light. Then to derive realistic performance, we also carried out the same calculation for any F, G, K and M main-sequence stars (667 targets) within 25pc with an optimal baseline of 80 m. In table 3, we show the full sample completude in the N band (assuming each star has an Earth-like planet in orbit). Earth-like planets are potentially detectable around 73% of nearby stars in that case.

The interferometer baseline has also an important impact on the detectivity. Figure 6 shows the completude of the sample (fraction of detected planets) as a function of the baseline and for several intensi-

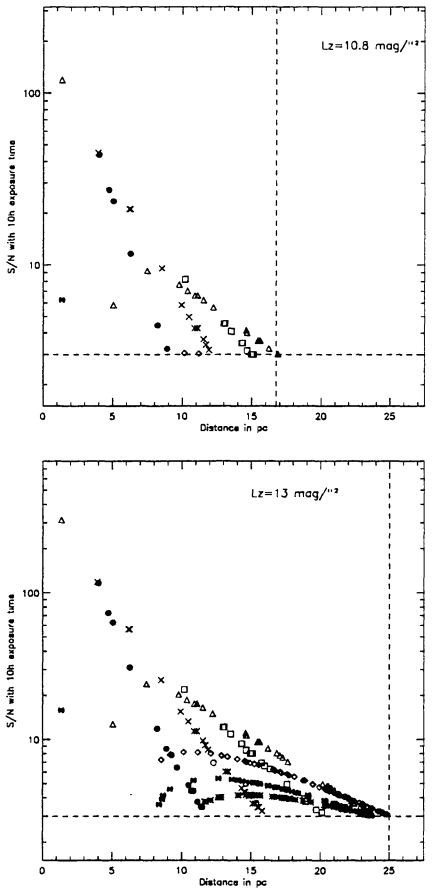

Figure 4. a : Signal to noise ratio obtained for the sample of Fig. 3 with a baseline of 80 m and a zodiacal flux of $10.8 mag/"^2$. *Earth-like planets are potentially detectable around 12 % of the stars (47 stars). The exo-zodiacal flux is 10 times brighter than the zodi. b : Signal to noise ratio obtained for the sample of Fig. 3 with a baseline of 80 m and a zodiacal flux of* $13.0 mag/"^2$. *Earth-like planets are potentially detectable around 67 % of the stars (262 stars).*

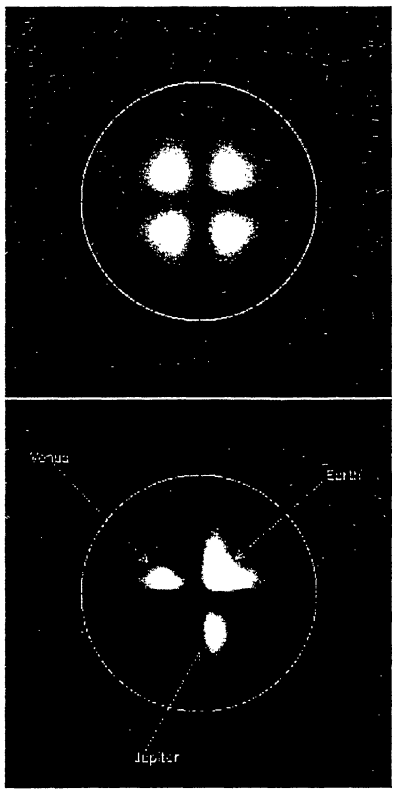

Figure 5. Coronagraphic images obtained with a 37 apertures hypertelescope. The simulation includes photon noise (T=10 hours, collecting area=10.6m², transmission=46%, star magnitude at 10μm=4.7), readout noise (5e⁻/pixel/frame), differential piston and tip-tilt errors between sub-apertures (λ/170rms) and mirror roughness (λ/170rms). The first image (left) is the coronagraphic image before subtracting the quadrants and results from a combination of 3 narrow bands ($8.4 \pm 0.75\mu m$, $10.2 \pm 0.75\mu m$ *and* $12 \pm 0.75\mu m$*). The Exo-Zodiacal light is dominant. The second image (right) shows Venus, the Earth and a secondary peak of Jupiter after subtracting opposite quadrants. The circle is the size of the Zero Order Field at* $10.2\mu m$.

Spectral type	F	G	K	M
number of stars	62	217	193	195
detectivity	45%	98%	80%	46%

Table 3. Detectivity for a full sample of stars (667) with 37 telescopes and an 80m baseline. The threshold is fixed to a signal to noise ratio greater than 3 and the exposure time is 10 hours. The zodiacal flux is 13 $mag/"^2$ *and exo-zodiacal flux is equal to 10 Zodi.*

ties of the zodiacal cloud. As the flux of the zodiacal light decreases the hypertelescope becomes obviously more sensitive to fainter stars, thus improving the sample completude. The dependance with the baseline is somewhat more complex and is correlated with the zodiacal flux. The number of positive detections reaches a maximum for an optimal baseline which depends on the zodiacal flux.

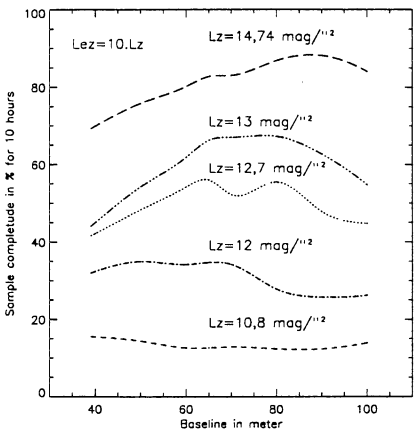

Figure 6. Percentage of detected Earth-like planets as a function of the baseline (ranging from 40m to 100m) and for a zodiacal flux of 10.8, 12.0, 12.7, 13.0, and 14.74 mag/"² ((Boulanger et Pérault 1988)).

For a fainter zodiacal flux (Boulanger et Pérault 1988) ($Lz = 14.74\ mag/"^2$), planets are becoming detectable around fainter stars, i.e. late-type stars or distant stars. However, late-type stars are most numerous and a larger baseline ($90m$) is then required to angularly separate the terrestrial planets. The maxima of the curves is then moving towards large baselines if the zodiacal flux decreases. For instance, with $Lz = 13 mag/"^2$, the maximum of detection is achieved for a baseline of $\sim 80m$ and for G-type and K-type stars. With a much brighter zodi ($Lz = 10.8 mag/"^2$) the curve is almost flat because only planets around the brightest stars are detected, which means F and G stars for small baselines ($\sim 40m$) and K and M nearby stars for large baselines ($\sim 100m$).

Figure 5 presents the result of numerical simulations using a FQ-PM to attenuate the central star, obtained with 37 telescopes, and 80 meters of baseline. Zodiacal and exo-zodiacal backgrounds are included in the image together with co-phasing defects and mirror roughness. The central G2V star ($m_v = 6.33$, $m_N = 4.70$) provides a photon flux of $1.64.10^6$ events/s in the N filter ($\lambda = 10.2 \pm 2.6 \mu m$) for a total transmission of 46%. Venus, the Earth, and Mars were added in the ZOF, Jupiter is added in the HOF. The luminosity of the zodiacal light is $L_z = 7.7.10^{-7} W/(m^2.sr.\mu m)$ corresponding to $14.07 - 13 - 12.5\, mag/"^2$ for respectively $8.4 - 10.2 -$ $12 \mu m$ As seen on Fig. 5, the FQ-PM provides a sufficient rejection rate, after substracting opposite quadrant, for the snapshot detection of Venus, the Earth and the dispersed peak of Jupiter with 37 subapertures in a total integration time of 10 hours. Mars would require a longer integration time (12 hours).

4. CONCLUSION

The new numerical simulation performed here confirm the capabilities of the hypertelescope with coronagraph concept to achieve exo-planet detection in the mid-IR. We find here that the dominant sources of noise when searching Earth-like planets in the mid-IR are the exo-zodiacal and zodiacal clouds. The stellar residuals, with the speckles generated by phase errors are fainter if the starlight rejection is larger than 10^5.
The main drawback, the field of view limitation, can be overcome if exo-planets are detected using their secondary dispersed peaks. This makes it unnecessary to vary the array size for zooming the image, as suggested before. One can define an optimal fixed baseline according to the most frequent stellar spectral types to be observed. For instance, with a baseline of $80m$ an Earth-like planet is potentially detectable around 73% of target stars in less than 10 hours. A subsequent step which we now prepare is the testing of a hypertelescope with a phase-mask coronagraph. A study with a miniature version of it for laboratory testing is under study.

REFERENCES

Boccaletti A., Riaud P., Moutou C. & Labeyrie A. 2000, Icarus 145, Vol 2, 628-636

Boulanger F. & Pérault M. 1988, ApJ 330, 964-985

Bracewell R.N. 1978, Nature 274, 780-781

Bracewell R.N. & McPhie R.H. 1979, Icarus 38, 136-147

The Hipparcos and Tycho Catalogues, 1997, ESA SP-1200

Labeyrie A. 1996, A&AS 118, 517-524

Roddier F., Roddier C., 1997, PASP 109, 815-820

Rouan D., Riaud P., Boccaletti A., Clénet Y, & Labeyrie A., 2000, PASP 112, 1479-1486

Riaud P., Boccaletti A., Rouan D., Lemarquis F., & Labeyrie A., 2001, PASP 113, 1145-1154

Riaud P., Gillet S., Labeyrie A., Boccaletti A. et al. 2001 Proc. "From Optical to Millimetric Interferometry", Liège Int. Astroph. Coll., p85-94